Probabilistic Engineering Mechanics 59 (2020) 103038

Contents lists available at ScienceDirect

Probabilistic Engineering Mechanics

journal homepage: www.elsevier.com/locate/probengmech

Soil deposit stochastic settlement simulation using an improved autocorrelation model

Qingxia Yue [a,*], Jingru Yao [b]

[a] School of Civil Engineering, Shandong Jianzhu University, Jinan, China
[b] Department of Civil Engineering, South China University of Technology, Guangzhou, China

ARTICLE INFO

Keywords:
Autocorrelation model
Linear-exponential-cosine function
Random field simulation
Differential settlement analysis

ABSTRACT

Soil parameters are spatially random variables. Thus, the spatial correlation relationship, besides the mean and variance, of a specific soil site is needed for any realistic stochastic modeling. In this regard, an improved autocorrelation model involving a linear, an exponential and cosine terms, named linear-exponential-cosine (LNCS), is adopted here to capture the spatial properties of the soil deposits. Further, a random field of the soil deposit is simulated using a two-dimensional Karhunen–Loéve expansion based on the new autocorrelation model. Furthermore, two cases for the soil settlement are calculated with the random field of the soil deposits. One case is the stochastic settlement from a reference paper. Some comparisons are undertaken, and it is found that the mean value agrees well with the reference. The other case involves the differential settlement analysis of a real engineering project. The settlement is calculated with the random field, the uniform field respectively, and is compared with the on-site measured values. The results show that the random field model can capture the differential settlement better than the corresponding uniform field model.

1. Introduction

Potential settlement calculation is of great interest in geotechnical engineering, especially for cases of non-uniform settlement. This is due to the fact that several problems may arise, such as cracking due to angular distortion, tilting due to differential settlement, and excessive downward displacement. All of these effects can be detrimental to the construction process, and excessive settlement can compromise the functional service or even the safety of the structure. Almost typically, the non-uniform settlement is caused by the inhomogeneous properties of the soil.

It is well known that soil deposits can be multi-layered with different kinds of soil. Therefore, it can be more accurate to consider the soil deposit by different soil type separately. Further, the soil parameters are spatially correlated. Thus, the mean and standard deviation are not adequate to capture the spatial correlation of the soil. In this context, the autocorrelation function (ACF) is used to capture the spatial correlated property, and the random field theory is adopted to describe the randomness and correlation of the soil [1,2]. Therefore, a proper and efficient autocorrelation function is one of the key parameters describing the spatial correlation. There have been many autocorrelation functions proposed and used in the soil deposit [3]. The autocorrelation has the feature that as the separation distance increases, the correlation reduces. Thus, the most commonly used is the simple exponential function [4], in which the autocorrelation value decreases asymptotically from one to zero as the distance increases.

In this paper, the soil deposits are studied according to different soil types. And a new correlation model, involving a linear, an exponential, and a cosine terms, named linear-exponential-cosine (LNCS), is adopted to simulate the spatial properties of the soil deposits. Further, the settlement of a soil deposit is calculated and analyzed based on the random field, which is simulated using a two-dimensional Karhunen–Loéve expansion relating to the new autocorrelation model. And the differential settlement of an engineering project is simulated and compared with the measured data. Settlement and differential settlement statistics predictions are carried out using Monte Carlo simulations combined with the deterministic finite element method (DFEM).

2. Improved autocorrelation model

2.1. ACF calculation and autocorrelation model

In the statistical analysis of the actual soil data obtained from field or laboratory tests, obvious ‘trends’ (changes in average values) are often encountered, most typically as a function of the depth. It is commonly accepted that the trends can be viewed as segments of a large-scale fluctuation, and a large-scale fluctuation must appear as part of the statistical characterization if the trend also exist on other site inference [5,6]. The choice of the trend to be removed is

* Corresponding author.
E-mail addresses: yueqx@sdjzu.edu.cn (Q. Yue), jingru503@qq.com (J. Yao).

https://doi.org/10.1016/j.probengmech.2020.103038
Received 16 January 2020; Accepted 29 January 2020
Available online 1 February 2020
0266-8920/© 2020 Elsevier Ltd. All rights reserved.

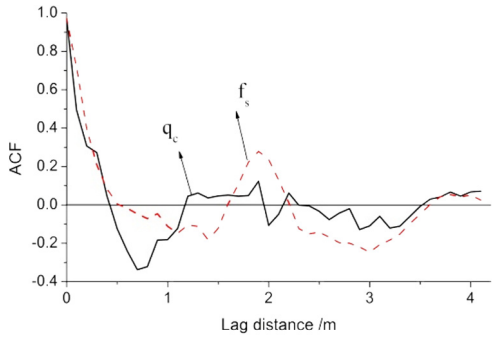

Fig. 1. A sample of the autocorrelation function.

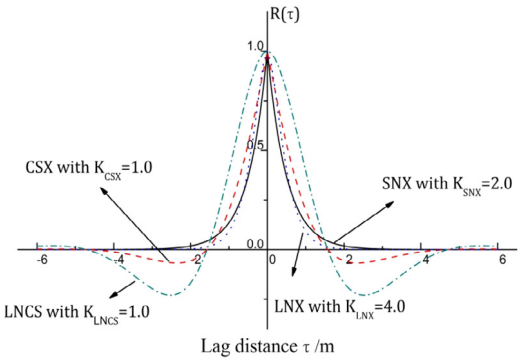

Fig. 2. The four autocorrelation models.

a delicate task as it affects the correlation structure, and the value of the statistical parameters describing the random field [7]. Linear trend removal has been used in several variability studies. However, from the field data considered, it is found that in the same soil layer, no apparent linear trend with the depth exists. In this case, it is advantageous to standardize the soil data by substituting each original datum point $q_c(z)$ by the equation

$$q(z) = \frac{[q_c(z) - \overline{q}_c]}{\tilde{q}_c}, \tag{1}$$

where $\overline{q}_c$ is the mean value of the layer soil, and $\tilde{q}_c$ is the standard covariance.

Next, the following procedures are adopted to obtain the ACF of the soil parameters.

For one of the samples, assume that $x_i = q_c(z_i)$ is the value of the sample at depth $z_i = i\Delta z$, $i = 1, 2, \ldots, n$. The sample covariance function is obtained from the moment estimator

$$C(\tau_j) = \frac{1}{n}\sum_{i=1}^{n-j}(x_i - \mu_x)(x_{i+j} - \mu_x), \tag{2}$$

where $j = 0, 1, 2, \ldots, n-1$, lag $\tau_j = j\Delta z$. Here, the mean value is expressed as

$$\mu_x = \frac{1}{n}\sum_{i=1}^{n} x_i. \tag{3}$$

The sample correlation is then

$$\rho(\tau_j) = \frac{C(\tau_j)}{C(0)}. \tag{4}$$

Proceeding with the calculations based on the above equations, the ACF of the soil data can be obtained.

Specifically, Fig. 1 is one sample of the autocorrelation curve from the cone penetration test data of a site in Shandong Province, China. It can be seen that as the separation (or lag) distance increases, the correlation decreases, although at large separations, where the numbers of data pairs are smaller, there is much statistical fluctuations. For zero separation distance, the correlation coefficient must equal 1.0. For a large separation distance, the correlation coefficient approaches zero. However, in between, the autocorrelation first falls from 1.0 to negative values and then becomes zero again. From the collected data of 157 soundings from Shandong Province of China, the same pattern can be found [8]. Moreover, many references about the autocorrelation curves also had such kind of feature [2,9]. To simulate the autocorrelation curve, various kinds of autocorrelation models have been employed in the geotechnical literature to fit ACF [5,7,10–12].

The most commonly used autocorrelation model (ACM) is the single exponential model (SNX).

$$R(\tau) = e^{-k_{SNX}\cdot|\tau|}, \tag{5}$$

where k_{SNX} is a parameter relating to the correlation length. However, this model is non-differentiable at the origin of the spatial axis. Thus, Spanos et al. [13] proposed a modified linear exponential model (LNX) by introducing a slight modification in the mathematical description of the single exponential model. In this context, the autocorrelation function becomes differentiable at the origin of the spatial axis. The expression for the LNX is

$$R(\tau) = (1 + k_{LNX}\,|\tau|)e^{-k_{LNX}\cdot|\tau|}, \tag{6}$$

where, k_{LNX} are the parameters that capturing the correlation length.

In Ref. [1], a "cosine-exponential" model (CSX) was used which can accommodate negative values of the ACF. The specific expression of the CSX is

$$R(\tau) = e^{-k_{CSX}\cdot|\tau|}\cos(k_{CSX}\,|\tau|). \tag{7}$$

Note that from the preliminary analysis of the autocorrelation of the soil data and many Refs. [2,4,8,9], it has been found that the autocorrelation value will change from positive to negative after a certain lag distance, and back to zero again. This means that the parameters change from positive correlation to negative correlation as the distance apart becomes larger. Further, note that even this model with alternating sign is not differentiable at the origin of the spatial axis. In this regard, the 'differentiability' of the model Eq. (6) and the alternating sign of model Eq. (7) are considered together. Thus, an improved autocorrelation model is used herein with linear, exponential, and cosine terms. It is named as linear-exponential-cosine model (LNCS), and it is expressed as

$$R(\tau) = (1 + k_{LNCS}\,|\tau|)e^{-k_{LNCS}\cdot|\tau|}\cos(k_{LNCS}\,|\tau|), \tag{8}$$

where k_{LNCS} is the corresponding parameter capturing the correlation length, which will be shown in Section 2.2.

Fig. 2 is a schematic diagram for the four autocorrelation models capturing their differences.

2.2. The correlation length of the LNCS model

Vanmarcke [3] has discussed the concept of the scale of fluctuation, δ, to measure the distance within which the soil property shows relatively strong correlation or persistence from point to point. This parameter can be calculated using the equation

$$\delta = 2\int_0^{\infty} R(\tau)d\tau. \tag{9}$$

Combining Eqs. (9) and (8), the scale of fluctuation of the different models can be obtained. Specifically,

$$\delta_{LNCS} = \frac{1}{k_{LNCS}}. \tag{10}$$

It is noted that often the concept of correlation length is used; it is given by the equation

$$c = \frac{1}{2}\delta. \tag{11}$$

3. Random field simulation with Karhunen–Loeve expansion

Next, the Karhunen–Loeve representation [14,15], often used to capture uncertainty in engineering applications, is used here for the simulation of the random field.

3.1. Basic concept of the Karhunen–Loeve expansion

A stochastic process $X(\tau,\theta)$ indexed on a bounded domain D, and having zero mean (for convenience) and finite variance, can be represented using a finite Karhunen–Loeve (K–L) series

$$X(\tau,\theta)=\sum_{i=1}^{\infty}\sqrt{\lambda_i}\xi_i(\theta)\phi_i(t), \tag{12}$$

where $\xi_i(\theta)$ is a set of uncorrelated standardized random variables with zero mean and unit variance. If $X(\tau,\theta)$ is a Gaussian process, then an appropriate choice of $\xi_i(\theta)$ is a vector of uncorrelated standard Gaussian random variables; $\{\phi_i\}$ and $\{\lambda_i\}$ are the eigenfunctions and eigenvalues of the covariance function $C(\tau_1,\tau_2)$, respectively. They satisfy the homogeneous Fredholm integral equation

$$\int_T C(s,t)\phi_i(t)dt=\lambda_i\phi_i(s). \tag{13}$$

The truncated version of $X(\tau,\theta)$ can be expressed as

$$X(\tau,\theta)=\sum_{i=1}^{M}\sqrt{\lambda_i}\xi_i(\theta)\phi_i(t). \tag{14}$$

The truncated Karhunen–Loeve expansion is optimal in the sense of a mean square error minimization [15].

The non-zero-mean stochastic process can be expressed as

$$X(\tau,\theta)=\mu+\sigma\sum_{i=1}^{M}\sqrt{\lambda_i}\xi_i(\theta)\phi_i(t). \tag{15}$$

For a particular application, the number of terms M to be chosen depends on the desired accuracy, and on the complexity of the autocorrelation function of the random field. Ordinarily, in most engineering applications, less than 10 terms suffice.

3.2. Two dimensional field simulation using Karhunen–Loeve expansion

Note that extension of the preceding developments to two dimensional field defined for the correlation function on a rectangular domain can be achieved, as well. For a certain class of covariance functions, which are separable, the eigenvalue and the eigenfunction for $X(\mathbf{t})$ are also separable. Thus, the random field can be expressed as truncated expression in the form

$$X(\mathbf{t})=X(t_1,t_2)=\sum_{k=1}^{N}\sqrt{\lambda_k}\phi_k(t_1,t_2)\xi_k\ , \tag{16}$$

where $\lambda_k=\prod_{j=1}^{d}\lambda_{i_j}^{(j)}$,

$$\phi_k(t_1,t_2,\ldots,t_d)=\prod_{j=1}^{d}\phi_{i_j}^{(j)}(t_j),\quad i_j\in N, 1\le i\le d,$$

d is the dimension.

4. Soil differential settlement analysis

4.1. Comparison study of field settlement

A model is used first to a simple foundation case. The model is from reference paper [16].

The model is a single footing of width 2.0 m to be founded on a soil layer of depth 10 m and length 30 m. The left and right boundaries are constrained with horizontal displacement, and the bottom boundary is fixed. The finite element model is shown in Fig. 3. The concentrated force acting on the rigid footing is simplified as uniform load 500 kN/m on the soil surface.

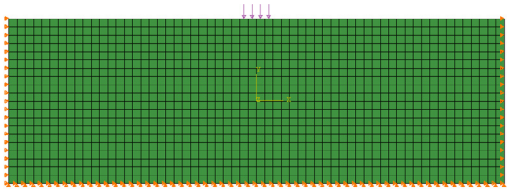

Fig. 3. The finite element model.

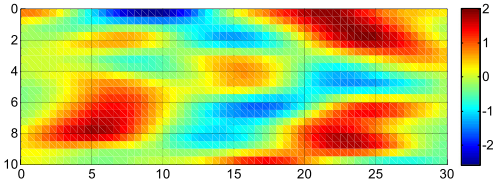

(a) Random field sample of $\ln E$

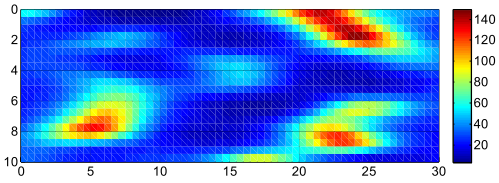

(b) Random field sample of elastic modulus

Figure 4. One random field sample

Fig. 4. One random field sample.

The elastic modulus is treated as a random field, and the lognormal distribution is adopted for the generation of the random field. The use of this distribution conform with the knowledge that the elastic modulus cannot have a negative value [17]. Accepting the use of this distribution, the elastic modulus field can be obtained through the transformation.

$$E_i=\exp(\mu\ln\varepsilon+\sigma_{\ln E}\cdot g_i) \tag{17}$$

where E_i is the elastic modulus of the element; g_i is the corresponding standard Gaussian random field; $\mu_{\ln E}$ and $\sigma_{\ln E}$ are the mean and standard deviation of lognormal E which can be obtained using the formulas

$$\sigma_{\ln E}^2=\ln(1+\sigma_E^2/\mu_E^2) \tag{18a}$$

and

$$\mu_{\ln E}=\ln(\mu_E)-\frac{1}{2}\sigma_{\ln E}^2 \tag{18b}$$

The mean value and standard deviation of the elastic modulus are 40 MPa and 40, respectively, which means the coefficient of variation is 1. It is assumed that the scale of fluctuation is $\theta_{\ln E}=3.0$ m. The Poisson ratio is taken as 0.25. Using the Karhunen–Loeve method, the random field can be obtained. Fig. 4 shows one sample of the random field of elastic modulus.

Considering the center point under the footing as the reference point; the settlement value can be obtained using the above finite element model. First, the mean value of the elastic modulus is adopted in the model; this case is defined as a uniform field. And then some stochastic simulation considering random field is done using the Monte Carlo Simulation (MCS). Here, 5000 times MCS are undertaken; and the mean value and the standard deviation can be estimated. The uniform field result, the random field results of mean value and standard

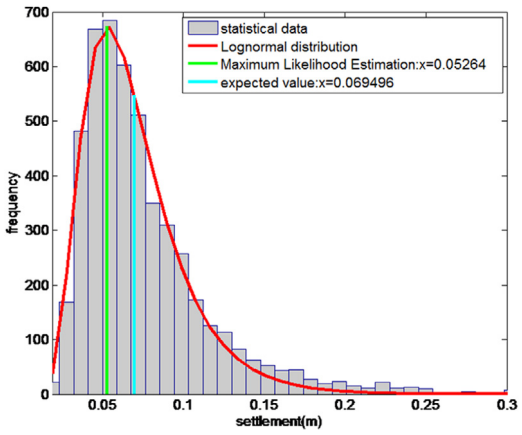

Fig. 5. Probability distribution of the settlement.

deviation are shown in Table 1, and the results from the Ref. [16] are also shown in Table 1. It can be seen that the random field related values are generally larger than the uniform field, which means that the settlement calculated using the uniform field may be unsafe.

Table 1
Settlement comparisons of the results.

Settlement	Uniform field (mm)	Random field (mm)	
		Mean value	Standard deviation
Calculated	36.7	69.5	56.2
Results from Ref. [16]	35.31	67.0	20.1

Fig. 5 shows the probability distribution of the settlement. It can be seen that the distribution of the settlement of the central point can be fitted by a logarithmic normal distribution, which conforms with the Ref. [16]. Further, the maximum likelihood estimation shows that the maximum estimation value of the settlement is 52.64 mm.

4.2. Differential settlement analysis of an engineering project

4.2.1. Introduction of the project

An 11-story residential building of concrete shear wall structure with raft foundation, shown in Fig. 6, located in Jiangsu province, China. After the building was completed, some differential settlement was detected, and the building leaned. It is found that the building leaning is mainly caused by the existence of soft substratum under the foundation. The soil profile is shown in Fig. 7, and the corresponding parameters for each soil layer are shown in Table 2. Note that the

(a) A picture of the building

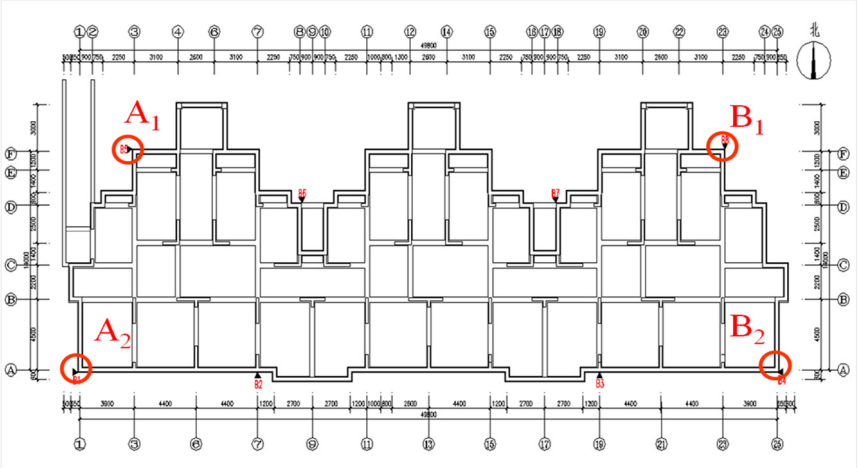

(b) Plan view of the building

Fig. 6. The residential building.

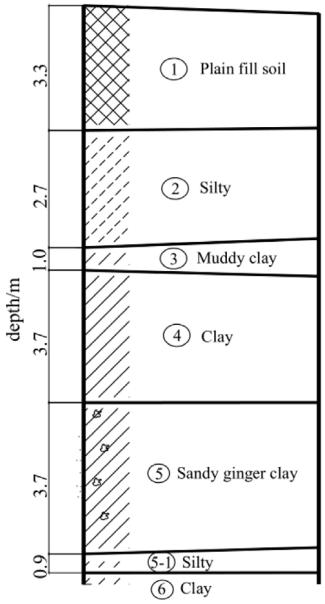

Fig. 7. Soil profile of the site.

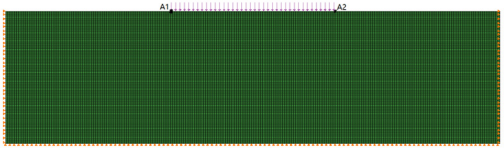

Fig. 8. Finite element model.

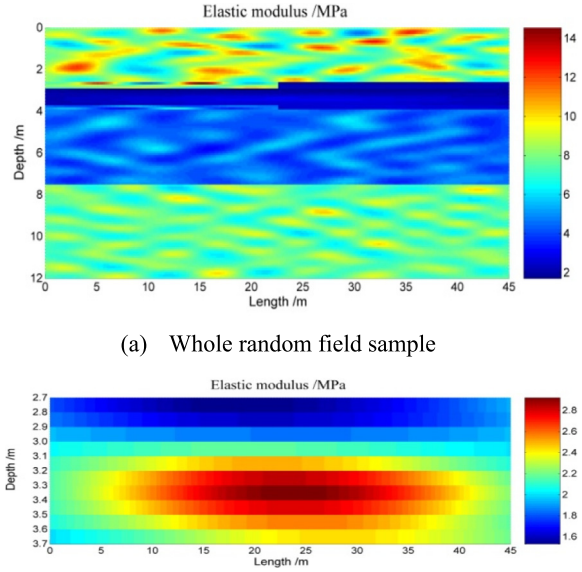

Fig. 9. One random field sample.

muddy clay layer thickness on the north and south is 1.0 m and 1.4 m, respectively, and the selfweight of the south is higher than the north; these factors mainly cause the differential settlement. The measured settlements on the north point (A1), and south point (A2) are 90.24 mm and 136.81 mm, respectively.

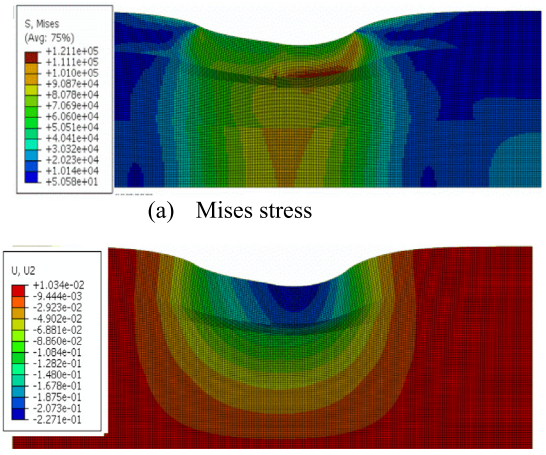

Fig. 10. The results of the uniform field.

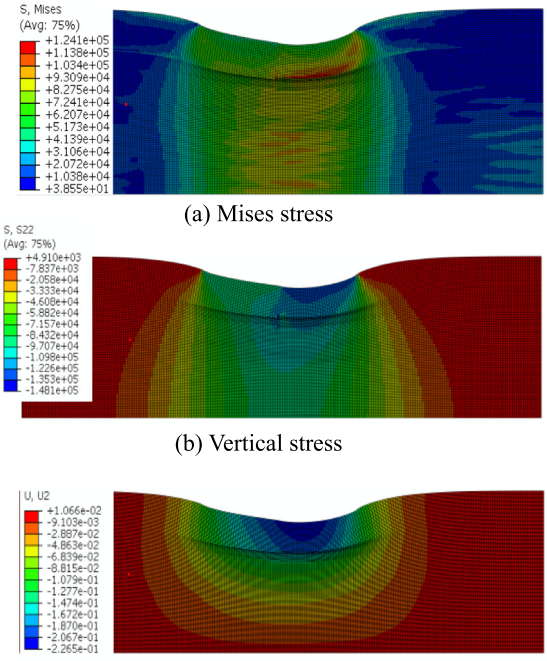

Fig. 11. The results of the random field.

4.2.2. *The finite element model*

A numerical simulation is conducted to calculate the differential settlement, and the random field is considered in the model. Fig. 8 shows the two dimensional finite element model, with size of 45 m × 12 m to minimize the boundary effect [18]. The left and right boundaries are constrained in the horizontal direction, and the bottom boundary is restrained in the vertical direction. The mesh sizes are 0.2 m and 0.1 m in the horizontal and the vertical directions respectively. The plane strain element model is adopted, and the elastic model is selected in the finite element analysis.

The soil elastic modulus, E, is treated as a random field, and the Poisson's ratio, μ, equals 0.25. The compressive modulus E_S usually determined in the engineering applications. The relation between the elastic modulus and the compressive modulus can be obtained by the

Table 2
Parameters of each soil layer.

Layer number	Soil type	North depth (m)	South depth (m)	Scale of fluctuation δ_v (m)	μ_{E_s} (MPa)	C.O.V (%)
②	Silty	2.7	2.5	0.163	10.05	0.22
③	Muddy clay	1.0	1.4	1.59	2.39	0.14
④	Clay	3.7	3.5	0.176	5.48	0.17
⑤	Sandy ginger clay	3.7	3.7	0.163	9.28	0.16
⑤-1	Silty	0.9	0.9	0.163	7.41	0.16

Table 3
Settlement results at representative points.

Points	Measured (mm)	Uniform field (mm)	Statistics of settlement of random field		
			Mean value (mm)	Standard deviation (mm)	C.O.V (%)
A1	90.24	94.54	96.82	2.45	2.53
A2	136.81	128.84	131.66	3.57	2.71

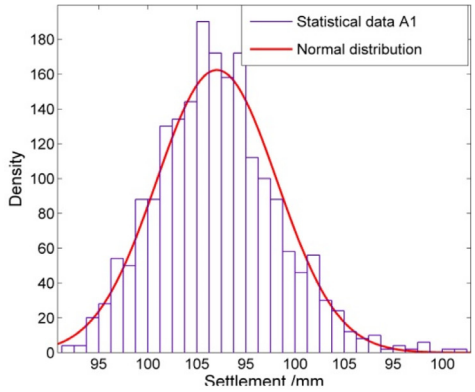

(a) Probability distribution of A1 settlement

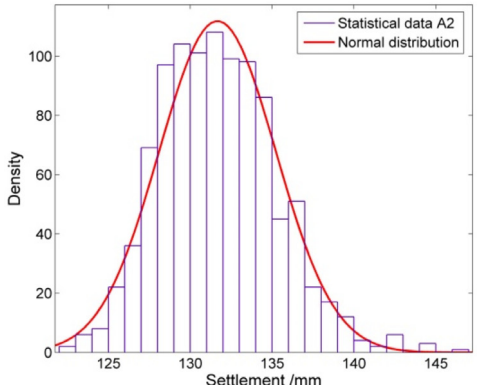

(b) Probability distribution of A2 settlement

Fig. 12. Probability distribution of settlement.

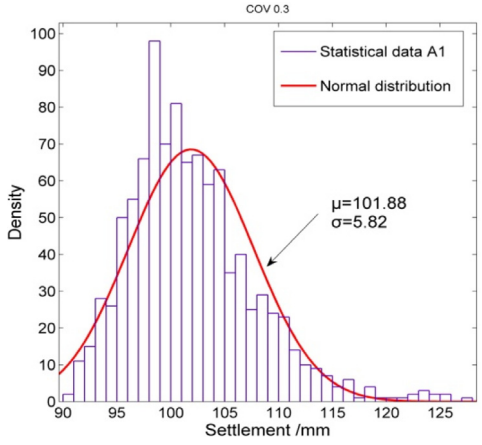

(a) Settlement distribution with COV 0.3

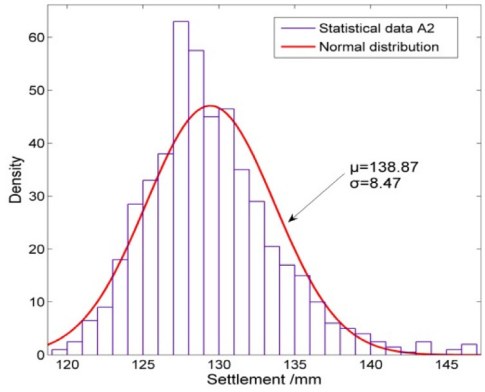

Fig. 13. Settlement distribution with different COVs.

equation

$$E = 1 - \frac{2\mu^2}{\mu(1-\mu)} E_s. \tag{19}$$

The raft foundation and the superstructure are simplified as distributed pressure acting on the soil surface within the length of 14.0 m, which equals the width of the foundation. Further, the load on the north half and the south half is calculated as 95 kN/m and 125 kN/m respectively.

Using the Karhunen–Loeve expansion method, and the autocorrelation function LNCS, the soil random field can be obtained. Note that in the natural site deposits, the correlation in the vertical direction tends to have much shorter distances than in the horizontal direction. A ratio of about one to ten for these correlation distances is common [19]. Here, the ratio of 10 is adopted. One sample of the random field is shown in Fig. 9(a). Obvious layer features can be seen from the figure. The muddy clay layer is much softer than the other layers, shown in Fig. 9(b). The midpoint discretization method is adopted, and in this case the values of the 'center' of elements are used to represent the random field.

4.2.3. Settlement simulation results

First, a uniform field, with the mean values, is calculated. Fig. 10 shows the results of the Mises stress and the settlement of the uniform soil field. It can be seen that the stress changes abruptly between the

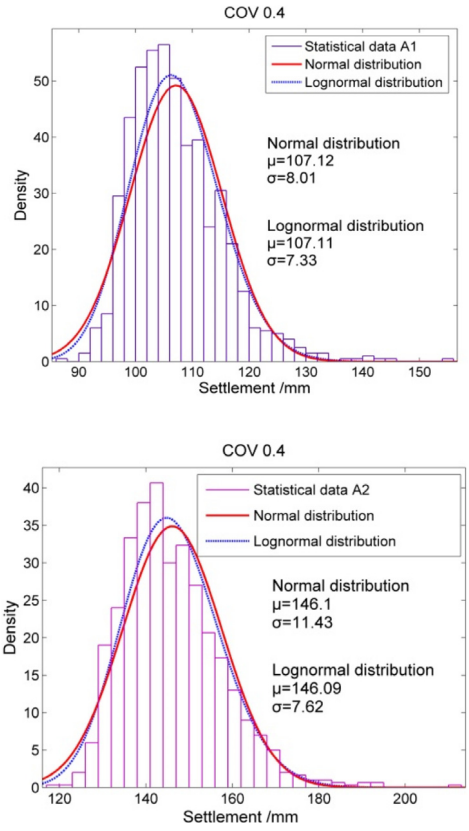

(b) Settlement distribution with COV 0.4

Fig. 13. (*continued*).

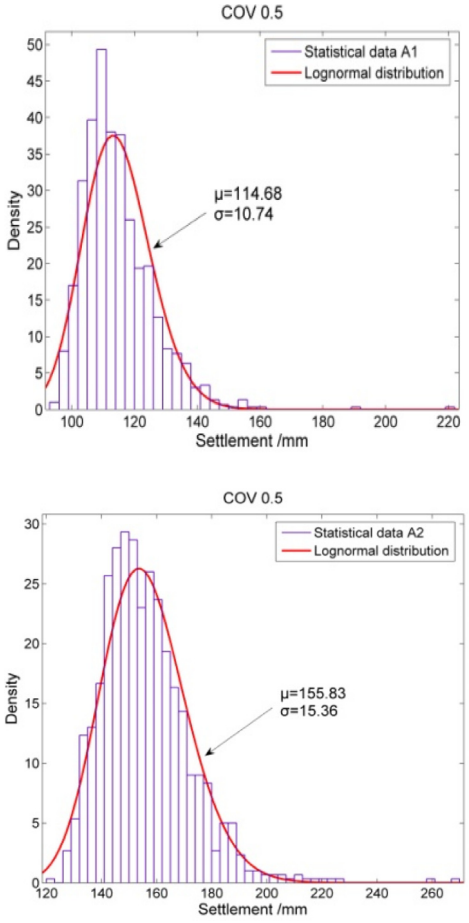

(c) Settlement distribution with COV 0.5

Fig. 13. (*continued*).

layers of soil, while in the random field the stress changes are more gradual (Fig. 11). From both figures, it can be seen that the differential settlement is due to the difference depth of the soft soil layer, and the load difference of the two sides.

Further, stochastic analysis is done using Monte Carlo simulation of 1000 times. To do this, 1000 random field samples of the elastic modulus of each layer soil are generated, and then the settlement analysis is done using the preceding model. Table 3 shows the settlement of the measured value, the result of the uniform field, and statistical results of the random field. It can be seen that the mean value of the random field is a somewhat higher than the uniform field for point A1, and smaller for point A2. Further, based on the "3σ" principle of normal distribution, the interval $(\mu - 3\sigma, \mu + 3\sigma)$ can be considered as the possible value interval of the random variable X in the actual problem, and its probability is $P\{|X - \mu| < 3\sigma\} = 99.74\%$. It can be seen that the measured settlement of point A1 (90.24 mm) is in the interval (89.47, 104.17) mm, and the A2 actual observed settlement 136.81 mm is also in the interval (120.95, 142.37) mm. This shows that the random field model can capture the differential settlement better than the corresponding uniform field model.

Fig. 12 shows a statistical graph and the probability density function curve of the normal distribution on the A1 and A2 settlements, respectively. Note that the normal distribution is adopted for this case.

4.2.4. Parametric analysis

The variation of the soil is significant. Thus, here different coefficient of variation 0.3, 0.4, and 0.5 of the soil are used. Fig. 13 shows the settlement distribution of point A1 and A2, indicated above. From Fig. 13 it can be seen that as the variation of soil parameters becomes higher, the settlement value calculated becomes larger. Further, as the variation becomes higher, the distribution of the settlement changes from more to a normal distribution to close to a lognormal distribution.

Also, the correlation length ratio of the horizontal and the vertical directions are examined here. To study the influence on different ratios of correlation distance for foundation settlements, the ratio n ($\delta_h/\delta_v = n$) changes from 10 to 90 are considered. The settlements of point A1 and A2 are obtained by the stochastic finite element analysis, shown in Fig. 14. Comparisons of random field settlement, uniform settlement, and the observed settlement are shown in the figure. It can be seen that as the ratio n becomes greater, the settlement becomes a somewhat higher, and the point A2 side is closer to the observed values.

5. Summary

An improved autocorrelation model (LNCS) has been adopted for the simulation of the random field in soil deposits. Related settlement has been calculated using the finite element method. Further, a stochastic analysis has been carried out for an engineering project considering the random nature of the local soil. The following concluding remarks can be made.

(1) The improved autocorrelation model can exhibit differentiability at zero lag, and alternating signs. Further, the random field can be efficiently represented using the Karhunen–Loeve expansion method in conjunction with the adopted autocorrelation model.

(2) Settlement calculation of two cases has been done; one case is from a cited reference, and the other pertains a real engineering project.

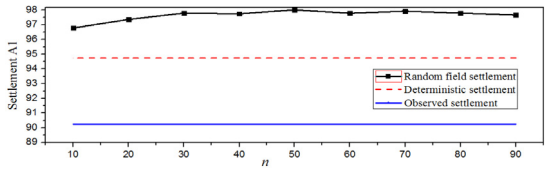

(a) Point A1 settlement

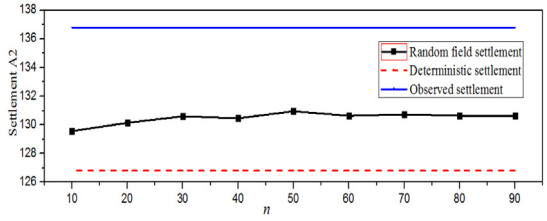

(b) Point A2 settlement

Fig. 14. Points A1 and A2 settlements with different ratios.

The results have shown that, in general, the random field can capture the character of the settlement better than the uniform field. Note that the probability distribution of the settlement is different for the two cases, and for the different coefficient of variations. Additional studies are clearly warranted to further elucidate this interesting problem of stochastic geotechnical engineering towards reliable physical and simultaneous efficient computing.

Acknowledgments

This research has been generously supported by the National Natural Science Funds of China (Grant No. 51878395 and 51678350), a Program for Changjiang Scholars and Innovative Research Team in Universities of China (No. IRT_17R69) which is gratefully acknowledged by the authors.

References

[1] E.H. Vanmarcke, Probabilistic modeling of soil profiles, J. Geotech. Eng. Div. ASCE 103 (11) (1977) 1227–1246.
[2] G.B. Baecher, J.T. Christian, Reliability and Statistics in Geotechnical Engineering, John Wiley & Sons, New York, 2003.
[3] E. Vanmarcke, Random Fields—Analysis and Synthesis, World Scientific, Singapore, 2010, revised and expanded new ed.
[4] C.N. Liu, C.H. Chen, Estimating spatial correlation structures based on CPT data, Georisk 4 (2) (2010) 99–108.
[5] D.J. DeGroot, G.B. Baecher, Estimating autocovariance of in situ soil properties, J. Geotech. Eng. ASCE 119 (1) (1993) 147–166.
[6] G. Fenton, Random field modeling of CPT data, J. Geotech. Geoenviron. Eng. 125 (6) (1999) 486–498.
[7] M. Uzielli, G. Vannucchi, K.K. Phoon, Random field characterisation of stress-normalised cone penetration testing parameters, Geotechnique 55 (1) (2005) 3–20.
[8] Q. Yue, J. Yao, H.-S.A. Ang, P.D. Spanos, Efficient random field modeling of soil deposits properties, Soil Dyn. Earthq. Eng. 108 (2018) 1–12.
[9] M.B. Jaksa, The Influence of Spatial Variability on the Geotechnical Design Properties of a Stiff, Overconsolidated Clay (Ph.D. dissertation), University of Adelaide, 1995.
[10] M.J. Spry, F.H. Kulhawy, M.D. Grigoriu, Reliability Based Foundation Design for Transmission Line Structures: Geotechnical Site Characterization Strategy, Report EL-5507(1), Electric Power Research Institute, Palo Alto, CA, 1988.
[11] S. Lacasse, F. Nadim, Uncertainties in characterizing soil properties, in: C.D. Shackleford, P.P. Nelson, M.J.S. Roth (Eds.), Uncertainty in the geologic environment: From theory to practice, ASCE Geotechnical Special Publication No.58, 1996, pp. 49–75.
[12] K.K. Phoon, S.T. Quek, P. An, Identification of statistically homogeneous soil layers using modified Bartlett statistics, Geotech. Geoenviron. Eng. 129 (7) (2003) 649–659.
[13] P.D. Spanos, M. Beer, J. Red-Horse, Karhunen–Loéve expansion of stochastic processes with a modified exponential covariance Kernel, J. Eng. Mech. 133 (7) (2007) 773–779.
[14] P.D. Spanos, R. Ghanem, Stochastic finite element expansion for random media, J. Eng. Mech. 115 (5) (1989) 1035–1053.
[15] R.G. Ghanem, P.D. Spanos, Stochastic Finite Elements: A Spectral Approach, Springer-Verlag, New York, 1991.
[16] G.A. Fenton, D.V. Griffiths, Probabilistic foundation settlement on spatially random soil, J. Geotech. Geoenviron. Eng. 128 (5) (2002) 381–390.
[17] G.A. Fenton, D.V. Griffiths, Three-dimensional probabilistic foundation settlement, J. Geotech. Geoenviron. Eng. 131 (2) (2005) 232–239.
[18] D.V. Griffiths, G.A. Fenton, Probabilistic settlement analysis by stochastic and random finite-element methods, J. Geotech. Geoenviron. Eng. 135 (11) (2009) 1629–1637.
[19] X. Li, K. Xie, Y. Yu, Research of the characteristic of correlation distance on soil properties indexes, China Civil Eng. J. 36 (8) (2003) 91–95 (in Chinese).